J. Min. Metall. Sect. B-Metall. 53 (3) B (2017) 303 - 308

Journal of Mining and Metallurgy, Section B: Metallurgy

MICROSTRUCTURE, HARDNESS AND INTERFACIAL ENERGY IN Co-9Al-10W-xNi (x=15, 25, 35 at. %) ALLOYS DURING AGING

C. Che, S. Yang, M. Wei, L. Zhang *, Q. Li, J. Gao, Y. Du

State Key Laboratory of Powder Metallurgy, Central South University, Changsha, Hunan, P.R. China

(Received 31 May 2017; accepted 04 September 2017)

Abstract

In the present paper, three Co-Al-W-Ni alloys (i.e., Co-9Al-10W-xNi with x=15, 25, 35 at. %) and their heat treatment mechanisms were carefully designed on the basis of the available phase equilibrium information. The temporal evolution of the microstructure and hardness in the Co-9Al-10W-xNi (x=15, 25, 35) alloys during aging process was measured, from which the effect of additional Ni contents, aging temperature and time on microstructure and hardness in the three Co-Al-W-Ni alloys was analyzed. Considering that the alloy compositions and heat treatment are not directly related with the hardness, the relationship between hardness and microstructure was then linked. It was found that the hardness of Co-based superalloys increases as the volume fraction of γ' precipitates increases, while decreases with the increase of the radius and interval of γ' precipitates. Moreover, the interfacial energy of γ/γ' interface was also evaluated on the basis of the coarsening kinetics of γ' precipitates and the Philippe-Voorhees model in combination with the thermodynamic and atomic mobility databases. The results indicate that the interfacial energies of γ/γ' interface reduce as the increase of additional Ni content and aging temperature.

Keywords: *Co-Al-W-Ni superalloys; Microstructure; Hardness; Coarsening; Interfacial energy.*

1. Introduction

With the development of the aerospace propulsion and land-based power generation, the temperature of combustion gas becomes higher and higher. It is an increasingly huge challenge to find one structural material that can withstand severe oxidizing environments and high operating temperature to meet more and more severe service environment. Currently, the most fascinating heat-resistant alloys are Ni-based superalloys strengthened by solid solution strengthening mechanism in *γ* phase and precipitation strengthening mechanism with *γ/γ'* coherent structure. However, there are two general problems during the development of new-generation Ni-based superalloys. On one hand, Ni-based superalloys usually contain more than 10 elements, and more new elements are to be added in order to increase their performance. For an alloy with so many elements, it is very complicated to achieve the quantitative description by using pure experimental studies. On the other hand, the temperature capability of Ni-based superalloys increases gradually, and almost approaches to the upper bound limited by the melting temperature [1, 2]. Thus, some new high-temperature alloys have been developing to replace Ni-based superalloys for the past years.

One exceptional representative is the new-generation Co-based superalloy, which starts from the Co-Al-W system found by Sato et al. [3]. In the new Co-Al-W based superalloys, the ternary compound $Co_3(Al,W)$ with $L1_2$ structure can coexist with a fcc solid solution. This type of microstructure is similar to that of Ni-based alloys, and thus those new Co-Al-W based superalloys show excellent mechanical properties. Since the melting temperature of Co is higher than that of Ni by 40 K, Co-Al-W based superalloys have a possibility to achieve a higher temperature capability than Ni-based superalloys [2, 3]. Moreover, such new Co-Al-W based superalloys usually contain 4~5 elements, which are much less compared with Ni-based superalloys [2]. Numerous investigations have been devoted to the investigation of microstructure [4, 5], alloy composition optimization [6, 7], partition of elements [6, 8], mechanical [9, 10] and physical properties [11, 12] of the new Co-Al-W-based superalloys. Among different topics during the development of high-performance Co-Al-W-based superalloys, the following two are of the central interest: one is the low γ′ solvus temperature, which limits the mechanical properties of Co-Al-W-based superalloys at higher temperature; while the other is the narrow *γ/γ′* two-phase region, which makes the optimization of alloy compositions difficult. As a result, a small fluctuation of

Dedicated to the memory of Professor Dragana Živković

* *Corresponding author: lijun.zhang@csu.edu.cn*

DOI:10.2298/JMMB170531021C

alloy composition in actual production may cause some harmful precipitations, which may reduce the mechanical properties of the alloy. One of the solutions to the above problems is the addition of alloying elements, such as Ta, Ti, Nb and Ni [8, 13]. Among all the alloying elements, addition of Ni can increase the γ' solvus temperatures continuously while keep the solidus temperature nearly unchanged [14]. Moreover, the addition of Ni can also broaden the γ/γ' two-phase region [13, 15].

Additionally, it is well known that the stability of this type of γ-γ' microstructure at elevated temperatures depends upon the resistance to coarsening of γ' precipitates, resulting in enhanced creep properties. Interfacial energies between γ and γ' phases play an extremely important role in controlling coarsening of γ' precipitates during aging process. Moreover, the interfacial energy, as an important thermo-physical parameter, is a prerequisite for quantitative simulation of microstructure evolution using such as the phase-field modeling [16-21]. However, there are few studies on interfacial energies of γ/γ' interfaces in Co-based superalloys except that Meher et al. [22] roughly evaluated one interfacial energy in Co-10Al-10W alloy based on their own experimental information. Up to now, there are several methods for estimating the interfacial energy, including first-principle calculations [23], molecular dynamics [24], Lifshitz-Slyozov-Wagner (LSW) theory [25, 26] and Kaptay's model [27]. The LSW theory is the most widely used method for studying the coarsening process of γ' and then evaluating interfacial energies by combining with the experimental coarsening information in superalloys. However, the application of the traditional LSW theory is limited by the following assumptions: (i) that only the dilute and ideal solution is applicable, (ii) that the alloy system is binary, and (iii) that the off-diagonal diffusivities are neglected, etc. [28]. There are several publications available in the literature [29, 30] to broaden the application scope of LSW theory. Very recently, Philippe and Voorhees [31] generalized the LSW theory into the multicomponent alloy by removing the above restrictions. One more nice thing in the model (i.e., P-V model) by Philippe and Voorhees lies in that with the real thermodynamic and atomic mobility databases can be coupled for providing the accurate composition and diffusivity information [31].

Consequently, a series of Ni-additional Co-9Al-10W alloys with different Ni contents and different aging processes will be designed on the basis of the available phase equilibrium information [13,14]. The effect of Ni on microstructure and hardness in the target Co-Al-W alloys during aging is to be explored by using a combination of experimental techniques. Moreover, the interfacial energy of γ/γ' phases in the Co-Al-W-Ni alloys will be evaluated using the P-V model in combination with the available thermodynamic [32] and atomic mobility [33, 34] databases, and the effect of Ni on interfacial energy of γ/γ' phases is thus to be investigated.

2. Experimental procedure

Co-9Al-10W-xNi (x=15, 25, 35, in wt. %) alloys were prepared from pure Co (purity: 99.98 wt. %), Ni (purity: 99.995 wt. %), Al (purity: 99.99 wt. %), and W (purity: 99.99 wt. %) by vacuum arc melting under a argon atmosphere. Small pieces of specimens were cut from the ingots and sealed in vacuum quartz tubes. All the samples were then annealed at 1573 K for 24 h in order to achieve the complete solid solution, followed by quenching in air. Subsequently the samples sealed in vacuum quartz tubes were subject to aging at 1123 K and 1223 K for 100h, 200h, and 300h respectively, followed by quenching in water.

Each specimen was mechanically ground and further polished. After being etched with the etchant of 66.7% HNO_3 +33.7% CH_3OH, the samples were observed using a Leica-DM4000M optical microscope. The microstructure of the aging samples was observed using Quanta FEG 250 secondary electron microscopy. The volume fractions of the γ' phase were measured by image analysis using an Image-Pro plus 6.0 metallographic analyzer. At least three different image views were obtained for each specimen. The Vickers hardness of the samples was measured by Buehler5104 microhardness tester, and each sample was tested for 5 times.

3. Results and discussion

3.1 Microstructure evolution

Fig. 1 (a) shows the typical dendritic structure of the cast Co-9Al-10W-35Ni alloy. It is obvious that the sizes of dendrites are different and their directions are slightly skewed due to the heat flow and the instability of external environment. The sample was investigated by XRD and the result indicated that γ and γ' phases exist in the as-cast alloys. After solution treatment, the typical microstructure of the Co-9Al-10W-25Ni alloy is shown as Fig. 1 (b). As is shown in the figure, the fine spherical particles of γ' precipitates homogeneously distribute in γ phase matrix. The γ' phase precipitates from γ matrix when the sample is quenched in air after solution treatment. Moreover, in the early stage of precipitation process, the particles of γ' phase are fine and sphere due to the effect of interfacial energy.

Fig. 2 shows the influence of additional Ni content, aging time and aging temperature on the microstructure of alloys during aging process. As can be seen in Fig. 2, one knows that the size of γ' phase increases as the aging time increases. Moreover, after a certain aging treatment, the morphology of γ' phase becomes more round as the additional Ni content increases in alloys. The morphology of γ' phase in the Co-9Al-10W-35Ni alloy aging at 1223 K is near-spherical. The possible reason lies in the competition between interfacial energy and elastic strain energy. It is well known that the lattice mismatch δ between γ phase and γ' phase is defined as $\delta=2\cdot(\alpha_{\gamma'} - \alpha_{\gamma})/(\alpha_{\gamma'} + \alpha_{\gamma})$, where α_{γ} and $\alpha_{\gamma'}$ are lattice parameters of γ phase and γ' phase respectively. Shinagawa et al. [13] found that with the

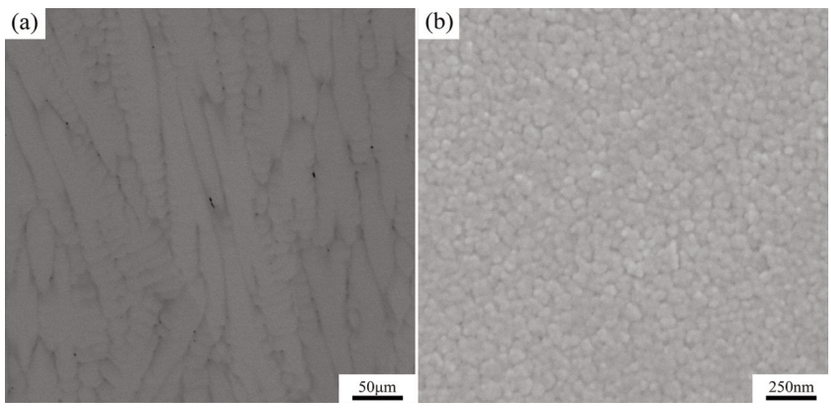

Figure 1. *(a) Backscatter image (BEI) of as-cast Co-9Al-10W-35Ni alloy (b) Secondary electron image (SEI) of the Co-9Al-10W-25Ni alloy after solution treatment*

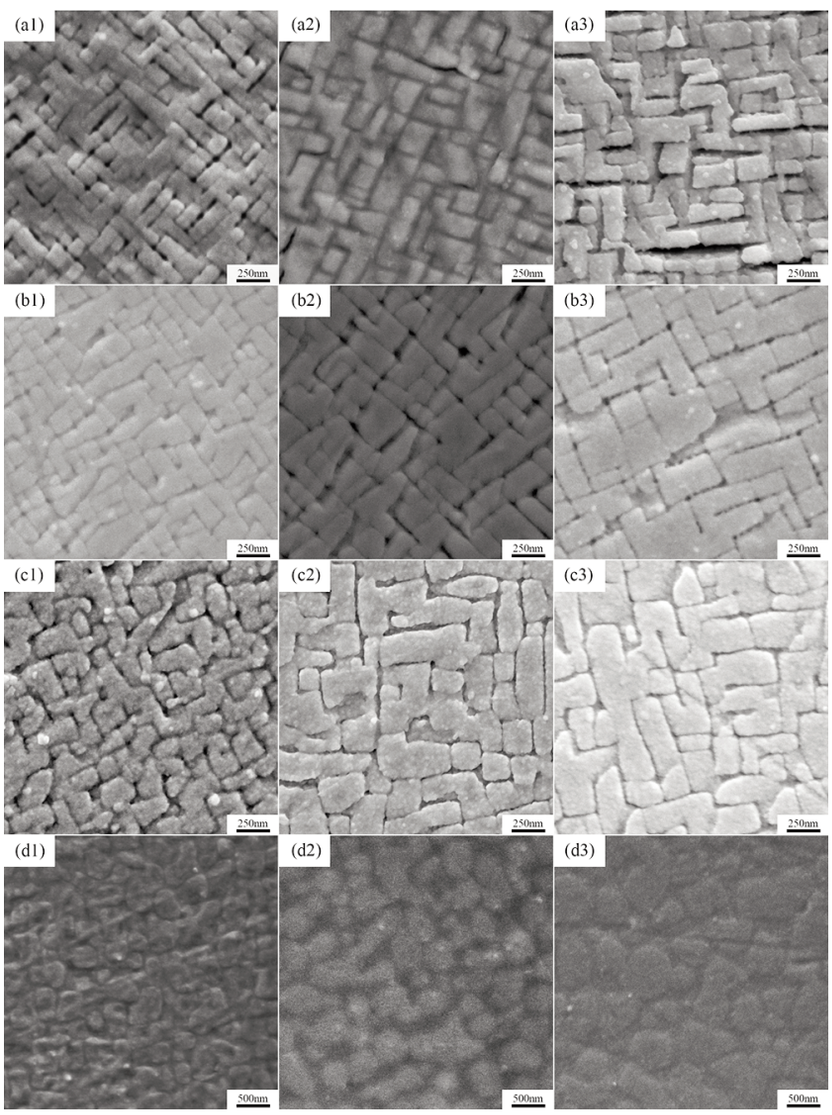

Figure 2. *SEIs of Co-9Al-10W-xNi (x=15, 25, 35) alloys after aging. (a1-a3) Co-9Al-10W-15Ni aging at 1123 K for 100h, 200h and 300h; (b1-b3) Co-9Al-10W-25Ni aging at 1123 K for 100h, 200h and 300h; (c1-c3) Co-9Al-10W-35Ni aging at 1123 K for 100h, 200h and 300h; (d1-d3) Co-9Al-10W-35Ni aging at 1223 K for 100h, 200h and 300h.*

increment of Ni content, W tends to distribute in the γ phase. Based on Vegard's law, this change decreases the mismatch of γ phase and γ' phase. Therefore the elastic strain energy becomes smaller and the interfacial energy is thus the dominant factor in determining the morphology of γ' phase. Thus, as the increase of Ni contents, the morphology of γ' phase becomes more round. As can also be seen in Fig. 2, as the aging temperature increases from 1123 K to 1223 K, the size of γ' phase becomes larger and the morphology of γ' phase becomes more round. One possible reason is that the diffusion rate of elements is faster at higher elevated temperature, which promotes the growth of particles. Besides, since the temperature increase leads to the decrease of mismatch between γ phase and γ' phase [35], the cubic degree of the morphology of γ' phase reduces.

Based on the above microstructure characterization, one can know that there exists typical dendritic structure in the as-cast alloy, while the solute segregation can be removed and the fine spherical particles of γ' phase precipitate after the solution treatment. During aging process, γ' phase grows gradually and different morphologies for γ' phase result from the competition between the interfacial energy and the elastic strain energy, which originates from the alloy compositions and heat treatment mechanisms.

According to Sato et al. [3], the cuboidal γ' phase precipitates align along the <001> directions in compliance with the minimum energy principle, and the 2D morphologies of γ' phase in experiments are always either square or rectangle [36, 37]. However, more interesting 2D morphologies can be observed for γ' phase in the present experiments, including triangle, rectangle, trapezoid and pentagon in i.e., Co-9Al-10W-25Ni alloy shown in Fig. 3 (a-d). According to the recent phase-field simulation in our research group [38], different 2-D morphologies observed in experiments may arise from 2-D cutting of the three-dimensional (3-D) crystals at random angles. In the present work, the demonstrations of 2-D cut of the 3-D cube at different angles are showed in Fig. 3 (e-h), which correspond nicely to the experimental observations.

3.2 Vickers hardness

In this work, the relationship of Vickers hardness to Ni content, aging time and aging temperatures was also studied, as shown in Fig. 4. One can see from Fig. 4 that as the aging temperature increases from 1123 K to 1223 K, the hardness of alloys decreases markedly. According to the X-Z plane in Fig. 4, it is also obvious that the hardness of alloys decreases as the increase of additional Ni contents. However, the relationship between Ni content and hardness is nonlinear, which indicates that one should pay attention to the microstructure of alloys. Following the Y-Z plane in Fig. 4, the relationship between the hardness and aging time is not so obvious either, and it can be seen that with the increase of aging time, the hardness of alloys decreases slightly. Considering that hardness is closely related to microstructure of the alloys, we further studied the relationship of hardness with the volume fraction, radius and particle interval of γ' phase in this work. As can be seen in Fig. 5, the hardness depends on the volume fraction, particle radius and particle interval of γ' phase. In general, the hardness increases with the increase of volume fraction of γ' phase (shown in the Y-Z plane of Fig. 5) while it decreases with

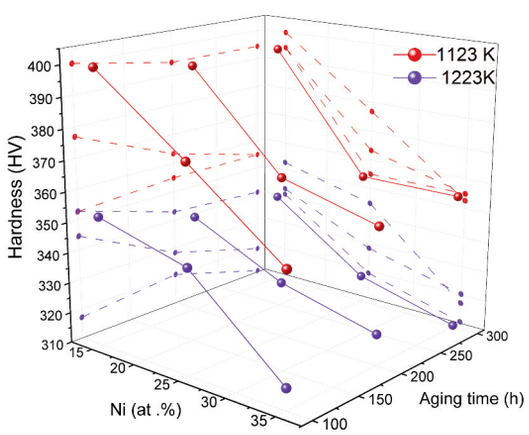

Figure 4. *Vickers hardness vs. additional Ni content, aging time and aging temperature. The red balls denote the experimental data aging at 1123 K while the blue balls represent those aging at 1223 K.*

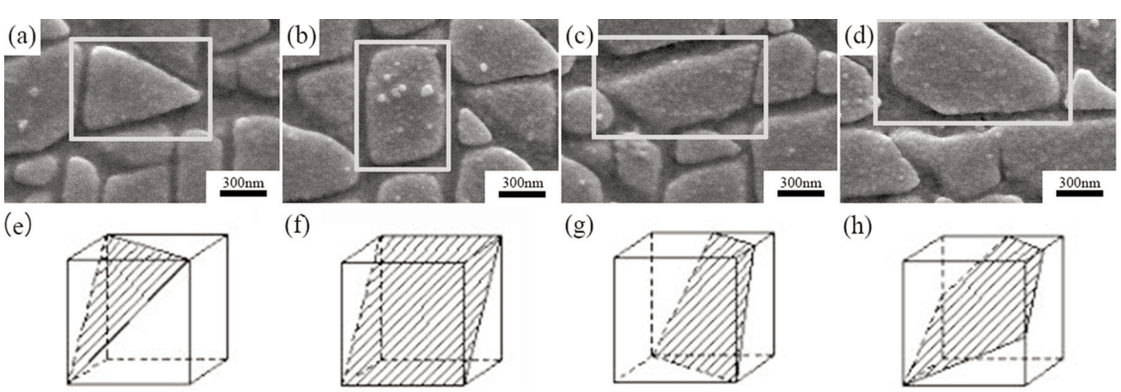

Figure 3. *SEIs for different two-dimensional morphologies of γ' phase in the Co-9Al-10W-25Ni alloy (a-d) and the cross-sections of cube (e-h).*

increase of the particle radius and particle interval of γ′ phase (shown in the X-Y plane of Fig. 5).

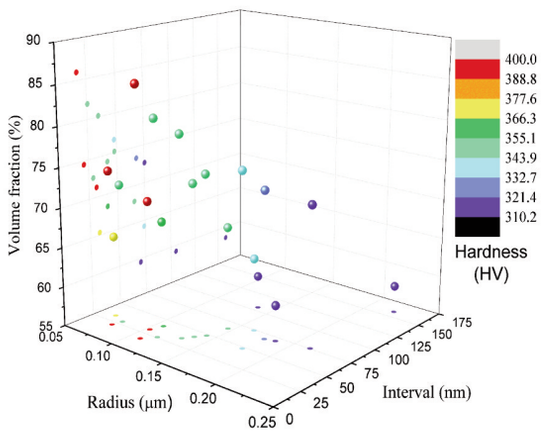

Figure 5. *Vickers hardness vs. volume fraction, radius and interval of γ′ phase.*

3.3 Interfacial energy of γ/γ′ phases

According to the P-V model [31], the temporal evolution of average precipitate size is as follows:

$$R(t)^3 - R(t=0)^3 = Kt \qquad (1)$$

where $R(t)$ and $R(t=0)$ are the mean particle sizes at time of t and at the beginning of the coarsening, respectively. While K is the coarsening rate constant.

The average particle sizes of γ' precipitates in the Co-9Al-10W-xNi (x=15, 25, 35) alloys after aging at two different temperatures (i.e., 1123 and 1223 K) with different aging time were counted by Image-Pro plus 6.0 metallographic analyzer. The cube of their sizes $R(t)^3$ against the aging time t is shown in Fig. 6. The slope of the line is exactly the coarsening rate constant. As shown in Fig. 6, the coarsening rates of γ′ precipitates increase as the content of Ni and aging temperature increase.

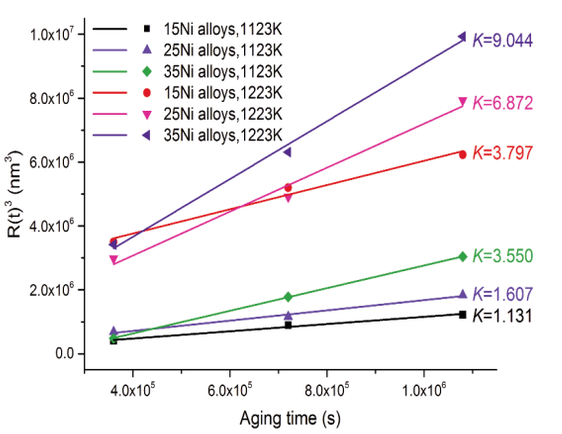

Figure 6. *$R(t)^3$ vs. the aging time t. The slopes of the lines are the coarsening rate constants while the unit of K is $10^{-27}m^3 \cdot s^{-1}$.*

According to the P-V model [31], K in Eq. (1) can be written as:

$$K = \frac{8V_m^{\gamma`}\sigma}{9(\Delta\overline{C})^T M^{-1}\Delta\overline{C}} \qquad (2)$$

where $V_m^{\gamma`}$ is the molar volume of the precipitate while $\sigma$ is the $\gamma/\gamma'$ interfacial energy. The vector $\Delta\overline{C} = x_i^{\gamma`} - x_i^{\gamma}$ for $i = 2\ldots N$, $x_i^{\gamma`}$ and x_i^{γ} are the equilibrium mole fractions of component i in the γ and γ' phases, respectively. M is the mobility matrix. The lattice parameter of the γ' precipitate in Co-Al-W-Ni alloys was reported by Shinagawa at al. [13] through the experimental measurements. In this work, the lattice parameter of the γ' precipitate was determined as 3.587Å and a molar volume of γ' precipitate was thus $6.95 \cdot 10^{-6}$ m^3·mol^{-1}.

The equilibrium mole fractions of components in this work were calculated by Thermo-Calc software [39] in combination with the Co-Al-Ni-W quaternary thermodynamic database by Zhu et al. [32]. The mobility parameters for Co, Al and W in the atomic mobility databases were taken from the work by Chang et al. [34] while those of Ni are due to the work by Campbell et al. [40]. The mobility matrix was then determined from the atomic mobility database established in the present work following our previous strategy [41].

The evaluated interfacial energies of γ/γ' phases in Co-9Al-10W-15Ni, Co-9Al-10W-25Ni alloys and Co-9Al-10W-35Ni alloys aging at 1123 K are 56.9, 42.6 and 38.7 mJ·m^{-2}, respectively. While the evaluated interfacial energies of γ/γ' phases in Co-9Al-10W-15Ni, Co-9Al-10W-25Ni and Co-9Al-10W-35Ni alloys aging at 1223 K are 5.0, 4.6 and 3.1 mJ·m^{-2}, respectively. The results are displayed in Fig. 7. Moreover, the calculated interfacial energy in Co-10Al-10W alloys at 1173 K and 1073 K due to Meher et al. [22] are 10 and 19 mJ·m^{-2} respectively, and their values are also superimposed in Fig. 7 for a direct comparison. As can be seen in Fig. 7, as the increase of additional Ni content and aging temperature, the interfacial energies of γ/γ' phase are reduced, which is reasonable in general. Moreover, considering the variations in alloy compositions and experimental conditions, the difference between the interfacial energy evaluated in the present work and the results due to Meher et al. [22] is also acceptable.

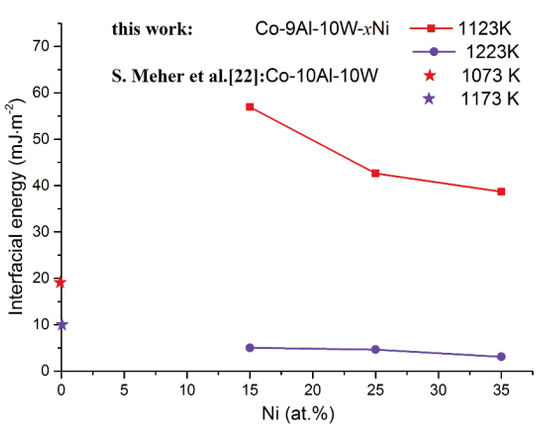

Figure 7. *Interfacial energies vs. additional Ni content at different aging temperatures.*

4. Conclusions

Based on the designed alloy compositions and heat treatment mechanisms, the microstructure and Vickers hardness in three Co-9Al-10W-*x*Ni alloys were measured. The effect of additional Ni contents on their microstructure and hardness were also analyzed.

The relationship between hardness and microstructure was then studied because the influence of alloy composition and heat treatment on hardness is not direct. The hardness of Co-based superalloys increases as the increase of the volume fraction of γ' phase while the decreases as increase of the particle radius and the particle interval of γ' phase.

The interfacial energy of γ/γ' interface was calculated by using P-V model in combination with the thermodynamic and atomic mobility databases. The interfacial energies of γ/γ' interface in Co-9Al-10W-15Ni, Co-9Al-10W-25Ni and Co-9Al-10W-35Ni alloys aging at 1123 K are 56.9, 42.6 and 38.7 $mJ{\cdot}m^{-2}$, respectively, while those aging at 1223 K are 5.0, 4.6 and 3.1 $mJ{\cdot}m^{-2}$, respectively. Moreover, as the increase of additional Ni content and aging temperature, the interfacial energies of γ/γ' interface are reduced.

Acknowledgement

The financial support from the National Natural Science Foundation of China (Grant Nos. 51301208, and 51429101) and the Hunan Provincial Natural Science Foundation for Youth of China (Grant No. 2015JJ3146) is acknowledged. Lijun Zhang acknowledges the project supported by State Key Laboratory of Power Metallurgy Foundation, Central South University, Changsha, China.

References

[1] M. Ooshima, K. Tanaka, N. L. Okamoto, K. Kishida, H. Inui. J. Alloys Compd., 508 (1) (2010) 71-78.

[2] E. A. Lass, M. E. Williams, C. E. Campbell, K.-W. Moon, U. R. Kattner. J. Phase Equilib. Diffus., 35 (6) (2014) 711-723.

[3] J. Sato, T. Omori, K. Oikawa, I. Ohnuma, R. Kainuma, K. Ishida. Science, 312 (5770) (2006) 90-91.

[4] S. Kobayashi, Y. Tsukamoto, T. Takasugi. Intermetallics, 19 (12) (2011) 1908-1912.

[5] M. Tsunekane, A. Suzuki, T. M. Pollock. Intermetallics, 19 (5) (2011) 636-643.

[6] M. Chen, C.-Y. Wang. Scripta Mater. , 60 (8) (2009) 659-662.

[7] L. Shi, J. J. Yu, C. Y. Cui, X. F. Sun. Mater. Sci. Eng., A, 635 (2015) 50-58.

[8] T. Omori, K. Oikawa, J. Sato, I. Ohnuma, U. R. Kattner, R. Kainuma, K. Ishida. Intermetallics, 32 (2013) 274-283.

[9] G. Feng, H. Li, S. S. Li, J. B. Sha. Scripta Mater. , 67 (5) (2012) 499-502.

[10] K. Shinagawa, T. Omori, K. Oikawa, R. Kainuma, K. Ishida. Scripta Mater., 61 (6) (2009) 612-615.

[11] L. Zhang, X. Qu, M. Qin, d. Rafi ud, X. He, Y. Liu. Mater. Chem. Phys., 136 (2-3) (2012) 371-378.

[12] C. H. Zenk, S. Neumeier, H. J. Stone, M. Göken. Intermetallics, 55 (2014) 28-39.

[13] K. Shinagawa, T. Omori, J. Sato, K. Oikawa, I. Ohnuma, R. Kainuma, K. Ishida. Mater. Trans. , 49 (6) (2008) 1474-1479.

[14] F. Xue, T. Mi, M. Wang, X. Ding, X. Li, F. Qiang. Acta Metall. Sinica 50 (7) (2014) 845-853.

[15] H. Y. Yan, V. A. Vorontsov, D. Dye. Intermetallics, 48 (2014) 44-53.

[16] N. Ta, L. Zhang, Y. Tang, W. Chen, Y. Du. Surf. Coat. Technol., 216 (2015) 364-374.

[17] M. Wei, Y. Tang, L. Zhang, W. Sun, Y. Du. Metall. Mater. Trans. A, 46 (7) (2015) 3182-3191.

[18] X. Yang, Y. Tang, D. Cai, L. Zhang, Y. Du, S. Zhou. J. Min. Metall. Sect. B-Metall., 52 (1) (2016) 77-85.

[19] J. Zhou, J. Zhong, L. Chen, L. Zhang, Y. Du, Z.-K. Liu, P. H. Mayrhofer. Calphad 56 (2017) 92-101.

[20] L. Zhang, M. Stratmann, Y. Du, B. Sundman, I. Steinbach. Acta Mater. , 88 (2015) 156-169.

[21] M. Akbarifar, M. Divandari. J. Min. Metall. Sect. B-Metall., 53 (1) (2017) 53-59.

[22] S. Meher, S. Nag, J. Tiley, A. Goel, R. Banerjee. Acta Mater. , 61 (11) (2013) 4266-4276.

[23] C. Woodward, A. van de Walle, M. Asta, D. R. Trinkle. Acta Mater. , 75 (2014) 60-70.

[24] J. J. Hoyt, M. Asta, A. Karma. Phys. Rev. Lett. , 86 (24) (2001) 5530-5533.

[25] I. M. Lifshitz, V. V. Slyozov. J. Phys. Chem. Solids 19 (1) (1961) 35-50.

[26] C. Wagner. Z. Elektrochem, 65 (1961) 581-591.

[27] G. Kaptay. Acta Mater. , 60 (19) (2012) 6804-6813.

[28] K. E. Yoon, R. D. Noebe, D. N. Seidman. Acta Mater. , 55 (4) (2007) 1159-1169.

[29] J. A. Marqusee, J. Ross. J. Chem. Phys., 79 (1) (1983) 373-378.

[30] A. J. Ardell, V. Ozolins. Nat. Mater. , 4 (2005) 309-316.

[31] T. Philippe, P. W. Voorhees. Acta Mater. , 61 (11) (2013) 4237-4244.

[32] J. Zhu, M. S. Titus, T. M. Pollock. J. Phase Equilib. Diffus., 35 (5) (2014) 595-611.

[33] C. E. Campbell, W. J. Boettinger, U. R. Kattner. Acta Mater. , 50 (2002) 775-792.

[34] H. Chang, G. Xu, X.-G. Lu, L. Zhou, K. Ishida, Y. Cui. Scripta Mater. , 106 (2015) 13-16.

[35] H. Mughrabi. Acta Mater. , 81 (2014) 21-29.

[36] H.-Y. Yan, J. Coakley, V. A. Vorontsov, N. G. Jones, H. J. Stone, D. Dye. Mater. Sci. Eng., A, 613 (2014) 201-208.

[37] F. Xue, H. J. Zhou, X. F. Ding, M. L. Wang, Q. Feng. Mater. Lett. , 112 (2013) 215-218.

[38] K. Wang, M. Wei, L. Zhang, Y. Du. Metall. Mater. Trans. A, 47 (4) (2016) 1510-1516.

[39] B. Sundman, B. Jansson, J.-O. Andersson. Calphad, 9(2) (1985) 153-190.

[40] C. E. Campbell, W. J. Boettinger, U. R. Kattner. Acta Mater. , 50 (4) (2002) 775-792.

[41] L. Zhang, Q. Chen. "CALPHAD-type modeling of diffusion kinetics in multicomponent alloys". In: Handbook of Solid State Diffusion (A. Paul and S. Divinski), Elsevier, Cambridge, 2017, p.321-362.